Chinese Chemical Letters 36 (2025) 110452

Contents lists available at ScienceDirect

Chinese Chemical Letters

journal homepage: www.elsevier.com/locate/cclet

Boron/phosphorus co-doped nitrogen-rich carbon nanofiber with flexible anode for robust sodium-ion battery

Jiaojiao Liang[a,*], Youming Peng[a], Zhichao Xu[a], Yufei Wang[a], Menglong Liu[a], Xin Liu[a], Di Huang[a,*], Yuehua Wei[b,*], Zengxi Wei[c]

[a] Hunan University of Technology, Zhuzhou 412008, China
[b] School of Physics and Optoelectronics, Xiangtan University, Xiangtan 411105, China
[c] Guangxi Key Laboratory of Petrochemical Resource Processing and Process Intensification Technology and School of Chemistry and Chemical Engineering, Guangxi University, Nanning 530004, China

ARTICLE INFO

Article history:
Received 8 July 2024
Revised 6 September 2024
Accepted 12 September 2024
Available online 12 September 2024

Keywords:
Co-doped
Flexible
Carbon nanofibers
Durable
Sodium-ion batteries

ABSTRACT

Flexible energy storage devices have been paid much attention and adapts to apply in various fields. Benefiting from the active sites of boron (B) and phosphorus (P) doping materials, co-doped carbon materials are widely used in energy storage devices for the enhanced electrochemical performance. Herein, B and P co-doped flexible carbon nanofibers with nitrogen-rich (B-P/NC) are investigated with electrospinning for sodium-ion battery. The flexible of binderless B-P/NC with annealing of 600 °C (B-P/NC-600) exhibits the remarkable performance for the robust capacity of 200 mAh/g at 0.1 A/g after 500 cycles and a durable reversible capacity of 160 mAh/g even at 1 A/g after 12,000 cycles, exhibiting the equally commendable stability of flexible B-P/NC-600. In addition, B-P/NC-600 delivers the reversible capacity of 265 mAh/g with the test temperature of 60 °C. More importantly, the flexible B-P/NC-600 is fabricated as anode for the whole battery, delivering the capacity of 90 mAh/g at 1 A/g after 200 cycles. Meanwhile, theoretical calculation further verified that boron and phosphorus co-doping can improve the adsorption capacity of nitrogen carbon materials. The favorable performance of flexible B-P/NC-600 can be ascribed to the nitrogen-rich carbon nanofibers with three-dimensional network matrix for the more active site of boron and phosphorus co-doping. Our work paves the way for the improvement of flexible anodes and wide-operating temperature of sodium-ion batteries by doping approach of much heteroatom.

© 2024 Published by Elsevier B.V. on behalf of Chinese Chemical Society and Institute of Materia Medica, Chinese Academy of Medical Sciences.

In recent years, lithium-ion batteries (LIBs) have been extensively studied and widespread used in everyday electronic devices due to its high specific capacity and stable cycle performance [1–3]. However, the limited reserves and increasing cost of lithium resources significantly hinders its development. As the same main group element, sodium-ion shows the similar physical and chemical properties [4–6]. Compared to lithium ions, the Stokes radius of sodium ions is smaller in organic solvent, suggesting that sodium ions have higher electrical conductivity [7]. Besides, the sodium also exhibits the advantage of low price and abundant reserves [8]. Based on the above reasons, sodium-ion batteries (SIBs) are considered as the potential secondary batteries in the sustainable development and costly effective.

As an important pole of sodium-ion battery, the selection of electrode material plays a vital role on the performance for SIBs [9]. Among the SIB's anode materials, carbon-based materials are superior than metals, transition metal compound, because of inexpensive, structurally stable and electrically conductive of carbon-based materials [10–12]. However, their capacity is insufficient, and to improve its sodium storage capacity, researchers have many outstanding optimization strategies, such as heteroatom doping, nanostructure and composite with other materials [13–16]. Up to now, heteroatom doping exhibits the excellent performance due to the simple and easy operation and the preferable properties. Typically, nitrogen (N), boron (B) and phosphorus (P) are commonly used for heteroatom doping in carbon-based materials. These doped heteroatoms can enter the carbon skeleton to affect the original carbon structure, thus impacting the physical and chemical properties of carbon-based materials. Compared to the single atom doping, multi-atom co-doping also utilized for the preparation of advanced electrode materials. For example, Yang and Shao reported that boron and nitrogen co-doped carbon nanospheres embodied better electrochemical performance for supercapacitors [17]. Meanwhile, there related theoretical calculations revealed that the for-

* Corresponding authors.
E-mail addresses: liangjiaojiiao@hut.edu.cn (J. Liang), dihuang@hut.edu.cn (D. Huang), yuehuawei@xtu.edu.cn (Y. Wei).

https://doi.org/10.1016/j.cclet.2024.110452
1001-8417/© 2024 Published by Elsevier B.V. on behalf of Chinese Chemical Society and Institute of Materia Medica, Chinese Academy of Medical Sciences.

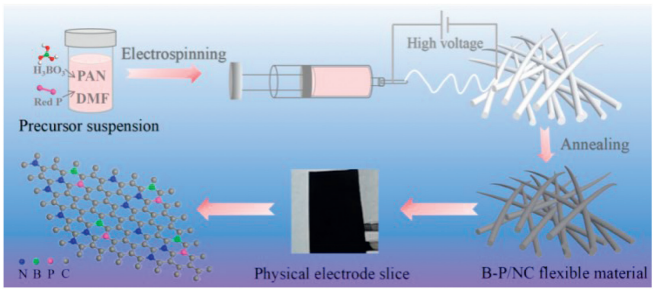

Fig. 1. The synthetic schematic diagram of flexible B-P/NC.

mation energy and the ionization energy of boron and phosphorus atom co-doping are much lower than that of single atom doping [18]. Furthermore, the introduction of heteroatoms can generate more active defect sites and increase the layer spacing, ultimately prompting the transfer of sodium ions and improving the cycle capability and rate performance [19].

In addition, as the requirement of wearable intelligent devices increased, the flexible energy storage materials have been gained the increasingly interests [20]. Multi-dimensional carbon nanofibers are considered as the preeminent substrates [21–23]. Benefiting the richer conductive network of multi-dimensional nanostructure, nanozation can reduce the transport distance of the charge, resulting in the outstanding electrochemical performance of electrode material. Typically, the most common, simple and convenient method of preparing multi-dimensional carbon nanofibers is electrospinning [24]. Moreover, the annealing temperature for electrode materials could impact on sodium storage capacity, rate performance and cycle stability [25,26]. Meanwhile, the wide-operating temperature of sodium-ion battery, which is important for the accommodate with the harsh environment in different temperature conditions should be thoroughly investigated [27].

In this work, the flexible and binderless B and P co-doped N-rich carbon nanofiber (B-P/NC) has been successfully fabricated with electrospinning and annealing. The sodium storage properties of flexible B-P/NC composite are explored with the temperature of 500 °C (B-P/NC-500), 600 °C (B-P/NC-600) and 700 °C (B-P/NC-700). And the flexible B-P/NC-600 exhibits remarkable capacity, better rate capability and durability cycle performance in sodium-ion battery. In addition, the electrochemical pseudocapacitance of B-P/NC is investigated and B-P/NC-600 exhibits more significant pseudocapacitance compared to B-P/NC-500 and B-P/NC-700. Meanwhile, B-P/NC-600 delivers the extraordinary properties of sodium storage with the wide-operating temperature and the prominent performance for the whole battery.

The synthetic process of flexible B-P/NC is displayed in Fig. 1. The precursor suspension of electrospinning is composed of polyacrylonitrile (PAN), *N*,*N*-dimethylformamide (DMF), H_3PO_3 and Red P with magnetic stirring. B and P atoms are co-introduced into the nitrogen-rich carbon nanofibers by the subsequent electrospinning and annealing process (including the pre-annealing in air and high temperature carbonization in Ar), successfully preparing the flexible B-P/NC materials. Correspondingly, XRD, Raman, SEM and TEM measurements are carried out to further study the structural information of the boron and phosphorus co-doped carbon nanofibers with nitrogen-rich (B-P/NC).

The XRD patterns in Fig. 2a exhibit a broad peak located at about 25° without other diffraction peaks, corresponded to the (002) planes of graphite carbon, which illustrates that the B-P/NC material still are graphite structure after B-P co-doping. In addition, it can be found that the intensity of diffraction peak has slightly enhanced associates with the annealing temperature, suggesting that high temperature is beneficial to form the ordered graphitized layer to enhancing the conductivity of materials [28]. To identify the formation of ordered graphitized carbon nanofiber, Raman spectrum was conducted. From the Raman spectra of Fig. 2b, it can be observed two typical Raman peaks locating at about 1360 and 1580 cm^{-1}, corresponding to D band and G band of carbon, respectively. Moreover, the intensity varies with respect to the annealing temperature of B-P/NC, and the intensity ratio of D and G bands of B-P/NC-700, B-P/NC-600 and B-P/NC-500 is 1.004, 1.170 and 1.270, respectively. The enhancement of I_D/I_G ratio manifests that carbon nanofibers are converted to the richest defect with decreasing annealing temperature, ultimately providing more active sites to store sodium ions [28,29]. Subsequently, the surface structure of the samples can be viewed in the SEM image of B-P/NC in Figs. 2c and d and Fig. S1 (Supporting information). Compared with the smooth distribution of B-P/NC-700, B-P/NC-600 and B-P/NC-500 display rougher surface to increase its surface area. Taking into account the conductivity and surface structure of the material, the co-doping carbon nanofibers annealing at 600 °C, which has better electrical conductivity, richest active defect sites and rougher surface, may be preferable performance for SIBs. As shown in Figs. 2e and f with the TEM image, there is no lattice fringes, indicating an amorphous graphite carbon for B-P/NC-600. The element distribution of B-P/NC-600 in Figs. 2g–k illustrates the uniformly nitrogen, boron and phosphorus elements distribution of carbon nanofibers, further identifying that the heteroatoms have been successfully incorporated into the B-P/NC-600.

The X-ray photoelectron spectroscopy (XPS) are characterized to analyze the specific electronic states of B-P/NC-600, and the low-resolution and overall view of XPS spectra are clearly observed with N, C and O, but B or P are barely observable in Fig. S2 (Supporting information). Whereas, the high-resolution XPS spectrum for C 1s, N 1s, B 1s and P 2p of B-P/NC-600 are shown in Fig. 3 and the corresponding content is 67.96%, 27.18%, 1.53% and 0.35%, respectively, suggesting the existing of B and P elements in the carbon nanofibers with rich nitrogen. The C 1s in Fig. 3a can be fitted with C–C/C=C peak (284.79 eV), C–C peak (284.58 eV), C–N peak (286.09 eV) and C–O peak (287.16 eV) [30–32], and the decomposed of N 1s spectrum in Fig. 3b is observed four components with pyridinic-N (398.26 and 398.32 eV), pyrrolic-N (400.05 eV) and graphitic N (401.4 eV) [33–36]. The B 1s spectrum in Fig. 3c could be fitted with two peaks at 190.37 and 192.01 eV, which ascribed to B-B and B-O [37,38], respectively. And the P 2p peak in Fig. 3d is divided into 133.8 and 132.33 eV, which corresponding to P-O and P-C [39,40].

In order to exploring the flexibility of B-P/NC-600, the schematic diagram of flexible anode by winding several rolls on the tweezers and then unrolling are shown in Fig. 4a, suggesting the favorable flexibility of B-P/NC-600 and the suitable candidate for flexibility anode. To detect the sodium storage property of the flexible B-P/NC-600, the CV curves in Fig. 4b are carried out to obtain the mechanism of storing sodium ions for the flexible B-P/NC-600 at 0.1 mV/s. The large peak at 0.5 V can be observed in the first cycle due to the reversible electrochemical adsorption and the irreversible formation of solid electrolyte interfaces (SEI) [41]. And another significant peak is found at 1.1 V possibly because of the reaction of Na^+ with functional group(s) at the surface of B-P/NC-600 [42]. Additionally, there is a weak cathode peak at 0.2 V, which is caused by the insertion of sodium ion [41]. In subsequent cycles, there is no significant REDOX peak, indicating that the B-P/NC-600 may be dominated by the pseudo-capacitor sodium storage mechanism, and the corresponding the galvanostatic charge-discharge curves are displayed in Fig. 4c. From the cycle performance at 0.1 A/g in Fig. 4d, the flexible B-P/NC-600 exhibits better stability with the capacity of 200 mAh/g for 500 cycles, while the flexible B-P/NC-700 and B-P/NC-500 only maintain the capacity of

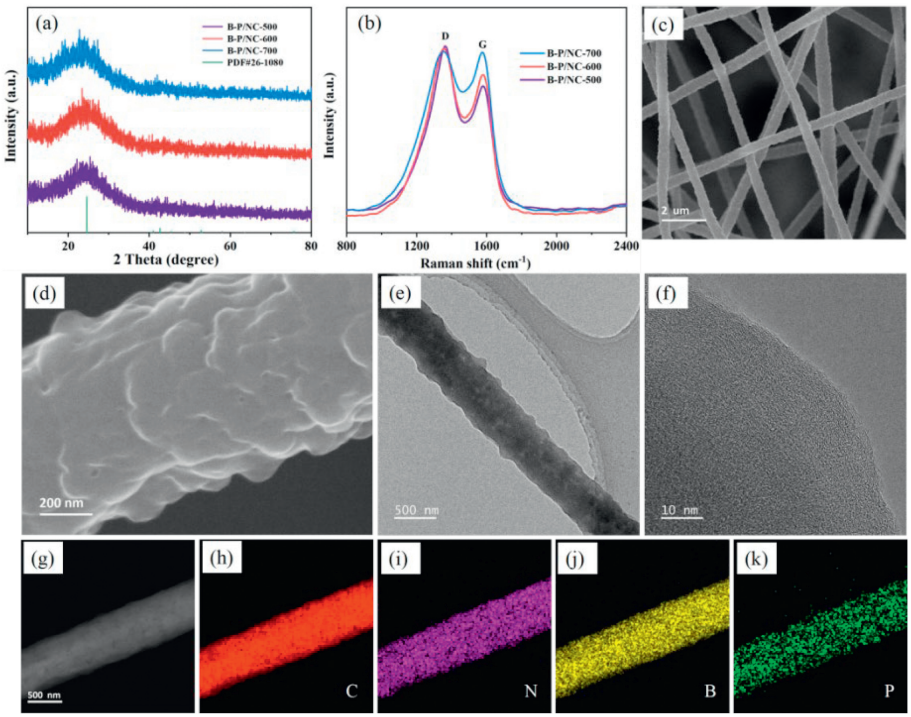

Fig. 2. (a) XRD patterns and (b) Raman spectra of B-P/NC. (c, d) SEM images and (e, f) TEM images of B-P/NC-600. (g–k) EDS element distribution mapping of individual nanofiber for B-P/NC-600.

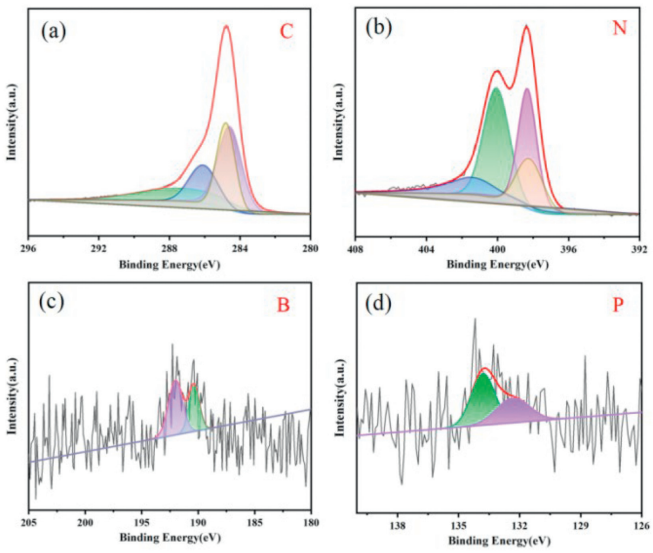

Fig. 3. The high-resolution XPS spectra of (a) C 1s spectrum; (b) N 1s spectrum; (c) B 1s spectrum and (d) P 2p spectrum.

140 and 120 mAh/g. This demonstrates the preferable sodium storage property of B-P/NC-600. Moreover, the rate capabilities of B-P/NC at various current densities are shown in Fig. 4e, the B-P/NC-600 exhibits the significantly higher capacities of 202, 178, 156, 136, 123, 103, and 78 mAh/g than that of B-P/NC-700 and B-P/NC-500 at the current density of 0.05, 0.1, 0.2, 0.5, 1, 2 and 4 A/g, respectively. Furthermore, the discharge capacity of B-P/NC-600 can be recovered to 183 mAh/g after the test current density again returned to 0.1 A/g, illustrating its general robust reversibility. The sodium storage capacity of flexible B-P/NC-600 with the stable capacity of 80, 125, 210 and 265 mAh/g as the test temperature at 0, 20, 40 and 60 °C are displayed in Fig. 4f. It is easy to find that the flexible electrode structure can be adapted to the temperature change without any affect on its sodium storage performance. In addition, the ultra-long cycle measurements at 1 A/g are applied for B-P/NC-600 to assess the cyclic durability are shown in Fig. 4g, and the initial discharge capacity is 335 mAh/g, and the discharge capacity stabilized at 160 mAh/g and coulomb efficiency maintain at 100% after 12,000 cycles at 1 A/g. Consequently, it can be mentioned that the B-P/NC-600 not only shows the excellent sodium storage performance in the flexible binderless electrode, but also exhibits the durable and robust of the cycle stability and width temperature work for sodium-ion battery.

To further study the electrochemical kinetics of sodium storage for B-P/NC-600, the CV curves are performed from 0.001 V to 2.5 V with a series of scanning rates from 0.2 mV/s to 2 mV/s (Fig. 5a), and the tendency of CV curves with the increase of scanning rate keeps almost unchanged, revealing the relatively low polarization for B-P/NC-600. Generally, the contribution of capacitive-controlled and diffusion-controlled could be divided into two parts of k_1v and $k_2v^{1/2}$ basing on the model of $i(v)=k_1v+k_2v^{1/2}$ (i is the current response, v is scanning rate, k_1 and k_2 is parameters) [22], and the contribution percentages ratio for capacitive-controlled approximately is to 73.7% at the scan rate of 0.6 mV/s by the calculation and analysis (Fig. 5b). Similarly, Fig. 5c displays the contribution percentages ratio with capacitive-controlled have been calculated to 64.8%, 69.6%, 74.8%, 76.5% and 84.7% with same analysis method, corresponding to other scanning rates at 0.2, 0.4, 0.8, 1.0 and 2.0 mV/s, respectively. In addition, the current response i and scanning rate v of CV can be described according to the mathematical model with $i=av^b$ ($0.5\leq b\leq 1$) and a, b of the model are the changeable parameters, which could be transformed into $\log(i)=\log(a)+b\log(v)$ with reasonable conversion. In addition, the b value close to 0.5 stands for a diffusion-controlled process and b value approach to 1 represents a capacitive-controlled behavior [43]. As displayed in Fig. 5d, the b value of the REDOX location is figured via the linear fitting to be 0.99, meaning that the main way of sodium-ion storage of the B-P/NC-600 comes from the

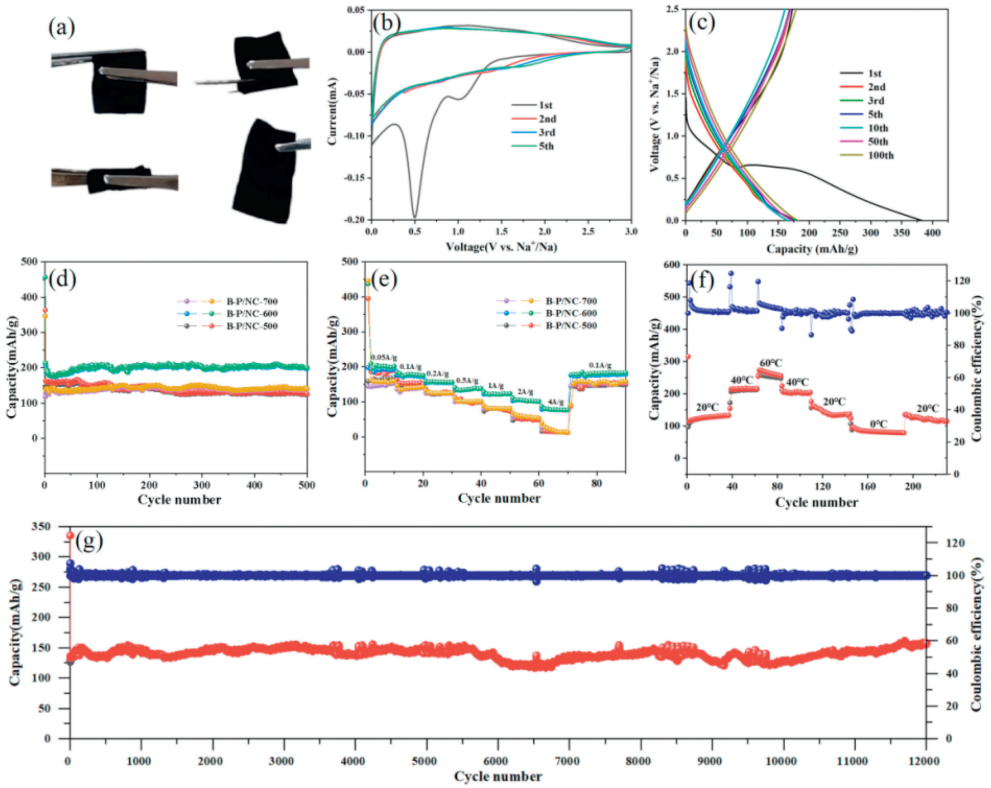

Fig. 4. (a) The schematic diagram of flexible B-P/NC-600 with different bending degree. (b) The CV curves at 0.1 mV/s and (c) galvanostatic charge/discharge curves at 0.1 A/g for B-P/NC-600. (d) Cycle performance at 0.1 A/g and (e) rate capabilities for B-P/NC anode. (f) Energy storage performance at different temperatures and (g) ultra-long cycle stability for B-P/NC-600 at 1 A/g.

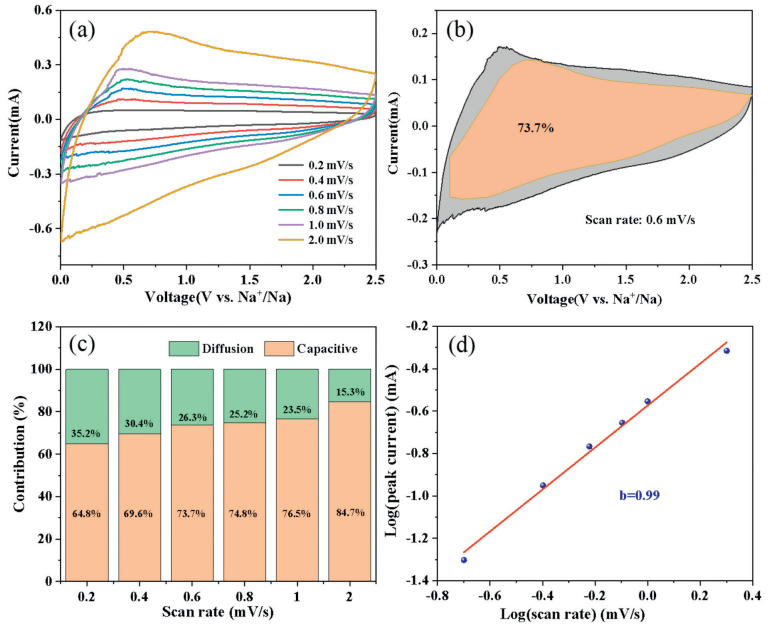

Fig. 5. (a) The CV curves with the 0.2–2.0 mV/s. (b) The CV outline of capacitive contribution at the scan rate of 0.6 mV/s. (c) The capacitive contribution percentage at different scan rates and (d) the plots of log(i) *vs.* log(υ) of for B-P/NC-600.

capacitive-controlled electrochemical characteristics. These results further indicate the less obvious REDOX peak in the CV curve for scanning rates of 0.1 mV/s.

Meanwhile, the CV curves at different scan rates from 0.2 mV/s to 2.0 mV/s for B-P/NC-500 and B-P/NC-700 are also characterized (Fig. S4 in Supporting information). To comparative investigate the capacitive-controlled sodium storage of B-P/NC anode, the electrochemical kinetics of sodium storage are shown in Table S1 (Supporting information). It can be known that the contribution percentages ratio with capacitive-controlled for B-P/NC-700 have been analyzed to 49.0%, 52.1%, 55.1%, 57.9%, 58.8% at the scanning rates at 0.2, 0.4, 0.6, 0.8, 1.0 and 2.0 mV/s and 74.8%, respectively, while it is 10.2%, 12.7%, 14.1%, 16.1%, 17.4% and 26.3% for B-P/NC-500. What is more, the b values for B-P/NC-500 and the

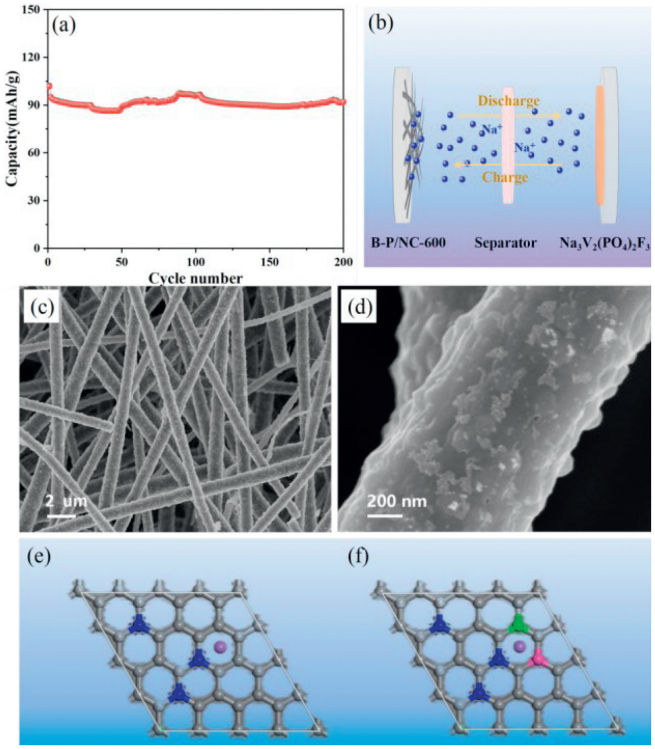

Fig. 6. (a) The cycle performance of B-P/NC-600 in whole cells at 0.1 A/g. (b) The schematic diagram of operating mechanism with the whole battery. (c, d) SEM images of B-P/NC-600 in whole cells after cycle. (e) Model of the pristine nitrogen-doped carbon materials adsorbing sodium. (f) Model of sodium adsorption on boron and phosphorus co-doped nitrogen-rich carbon materials.

B-P/NC-700 are 0.84 and 0.93 by the linear fitting, respectively, suggesting co-contribution of the both capacitive-controlled and battery-controlled behaviors of B-P/NC-500 and B-P/NC-700. Thus, the main contribution of capacitance characteristics in B-P/NC-600 might be response for more remarkable sodium storage performance and the excellent stability for ultra-long cycle performance at the large current. Overall, the robust and durable performance of binderless sodium-ion batteries could be better electrical conductivity and more active site of nitrogen-rich carbon nanofibers with co-doped B and P to form the flexibility of richer conductive network.

In order to further investigate the sodium storage properties of flexibility B-P/NC-600, the property of the whole battery composed of $Na_3V_2(PO_4)_2F_3$ cathode is investigated at the voltage window of 0.001 V to 4.2 V. The cycle performance of B-P/NC-600 in Fig. 6a illustrates that the capacity is reserved 90 mAh/g after 200 cycles in the whole battery at 1 A/g. To further explore the morphology and structure variation, the B-P/NC-600 of whole battery after circulation is disassembled and cleaned for the observation of SEM in Figs. 6c and d. The full view of B-P/NC-600 in Fig. 6c reveals the unabridged of three-dimensional network structure after the charge and discharge process. The high-resolution SEM in Fig. 6d is seen the unchangeable surface and diameter of the flexibility B-P/NC-600 except for some residual electrolytes, suggesting the stable structure and good storage capacity of sodium ions for B-P/NC-600 during cycling of whole battery. And the operating mechanism schematic diagram of the whole battery is displayed in Fig. 6b based on the above SEM results and test performance. The binderless B-P/NC-600 can bond directly with sodium ions, which provided by $Na_3V_2(PO_4)_2F_3$ during the repeated charge and discharge process. Furthermore, the detailed interactions and binding strength between sodium ions with the surfaces of pristine nitrogen-doped carbon materials (NC) and boron-phosphorus co-doped nitrogen-rich carbon materials (B-P/NC) are investigated and calculated with Materials Studio. Figs. 6e and f display the model of sodium ion sites adsorbed with NC and B-P/NC, and the obtained E_s is calculated −0.11 eV and −0.26 eV with the formula of $E_s = E_{G+Na} - E_G - E_{Na}$, corresponding to the adsorption energy of sodium ion for the NC and B-P/NC, respectively. By comparing the adsorption energies of the two models, it can be concluded that the method of changing the electronic properties of nitrogen-rich carbon materials by doping with boron and phosphorus atoms can improve the adsorption strength of nitrogen-rich carbon nanofibers for sodium ion. All these demonstrated that the simultaneous introduction of boron and phosphorus atoms can enhance the sodium-ion storage performance of nitrogen-rich carbon nanofibers.

In summary, the flexible anodes of boron/phosphorus co-doped nitrogen-rich carbon nanofiber without binder are prepared by electrospinning and annealing. The as-synthesized flexible and binderless B-P/NC-600 displayed robust and durable cycle performance of sodium ion storage with reversible capacity for 200 mAh/g at 0.1 A/g after 500 cycles and 160 mAh/g at 1 A/g after 12,000 cycles. Furthermore, the flexible B-P/NC-600 exhibits the outstanding rate performance with sufficient pseudo-capacitance characteristics. More importantly, the flexible B-P/NC-600 delivers the favorable sodium storage performance in wide area temperature and the outstanding whole sodium-ion battery performance with $Na_3V_2(PO_4)_2F_3$ cathode. The theoretical calculation also reveals the boron and phosphorus co-doping can enhance the ability to adsorb sodium ions for nitrogen carbon materials. At all, this work provides the novel approach of the double element doping and flexible anode with carbon material for the prominent performance of sodium-ion battery.

Declaration of competing interest

The authors declare that they have no known competing financial interests or personal relationships that could have appeared to influence the work reported in this paper.

CRediT authorship contribution statement

Jiaojiao Liang: Writing – review & editing, Writing – original draft, Resources, Project administration, Methodology, Investigation, Funding acquisition, Formal analysis, Data curation, Conceptualization. **Youming Peng:** Writing – original draft, Methodology, Investigation, Formal analysis, Data curation. **Zhichao Xu:** Writing – original draft, Investigation, Data curation. **Yufei Wang:** Methodology, Investigation, Funding acquisition, Formal analysis. **Menglong Liu:** Methodology, Funding acquisition. **Xin Liu:** Investigation. **Di Huang:** Writing – review & editing, Methodology, Funding acquisition, Conceptualization. **Yuehua Wei:** Writing – review & editing, Resources, Methodology, Funding acquisition. **Zengxi Wei:** Software, Resources.

Acknowledgments

This work is supported by Natural Science Foundation of China (No. 6230031623), the Natural Science Foundation of Hunan Province (No. 2024JJ5127), the Education Department of Hunan Province (No. 22B0580), the Scientific Research and Innovation Foundation of Hunan University of Technology (No. CX2317) and the Innovation and Entrepreneurship Training Project for College Students (No. S202311535061).

Supplementary materials

Supplementary material associated with this article can be found, in the online version, at doi:10.1016/j.cclet.2024.110452.

References

[1] J. Zhang, H. Zhang, S. Weng, et al., Nat. Commun. 14 (2023) 2211.
[2] H. Zhao, J. Li, Q. Zhao, et al., Electrochem. Energy Rev. 7 (2024) 11.
[3] N. Sharmili, R. Nagi, P. Wang, J. Energy Storage 68 (2023) 107622.
[4] D. Huang, D. Wu, J. Zhu, et al., Chin. Chem. Lett. 34 (2023) 107416.
[5] Y. She, X. Li, Y. Zheng, et al., Energy Environ. Mater. 7 (2023) e12538.
[6] T.T. Wei, X. Liu, S.J. Yang, et al., J. Energy Chem. 80 (2023) 603–613.
[7] E.J. Kim, P.R. Kumar, Z.T. Gossage, et al., Chem. Sci. 13 (2022) 6121–6158.
[8] T. Liu, Y. Yang, S. Cao, et al., Adv. Mater. 35 (2023) e2207752.
[9] S. Qiao, Q. Zhou, M. Ma, et al., ACS Nano 17 (2023) 11220–11252.
[10] H. Hou, X. Qiu, W. Wei, et al., Adv. Energy Mater. 7 (2017) 1602898.
[11] R. Zhao, N. Sun, B. Xu, Small Struct. 2 (2021) 2100132.
[12] T. Wu, M. Jing, L. Yang, et al., Adv. Energy Mater. 9 (2019) 1803478.
[13] Z. Song, M. Di, S. Chen, et al., Chem. Eng. J. 470 (2023) 144237.
[14] Q. Shi, K. Chen, Z. Yu, et al., J. Alloys Compd. 902 (2022) 163812.
[15] H. Zhang, Y. Huang, H. Ming, et al., J. Mater. Chem. A 8 (2020) 1604–1630.
[16] S. Zhao, Z. Guo, J. Yang, et al., Small 17 (2021) e2007431.
[17] Y. Yang, Z. Shao, Nanotechnology 33 (2022) 185403.
[18] K. Fan, K. Tang, M. Zhang, et al., Comput. Mater. Sci. 222 (2023) 112113.
[19] N. Ahmad, N. Muhammad, H. Chen, et al., J. Colloid Interface Sci. 650 (2023) 1725–1735.
[20] L. Kong, C. Tang, H.J. Peng, et al., SmartMat 1 (2020) e1007.
[21] J. Liang, C. Yuan, H. Li, et al., Nanomicro Lett. 10 (2018) 21.
[22] J. Liu, J. Liang, C. Wang, et al., J. Energy Chem. 33 (2019) 160–166.
[23] Z. Abbas, N. Hussain, S. Kumar, et al., Nanoscale 16 (2024) 868–878.
[24] H. Liao, W. Zhong, T. Li, et al., Electrochim. Acta 404 (2022) 139730.
[25] R. Guo, C. Lv, W. Xu, et al., Adv. Energy Mater. 10 (2020) 1903652.
[26] D. Chen, W. Zhang, K. Luo, et al., Energy Environ. Sci. 14 (2021) 2244–2262.
[27] Z. Li, Y. Zhang, J. Zhang, et al., Angew. Chem. Int. Ed. 61 (2022) e202116930.
[28] Z. Wu, B. Johannessen, W. Zhang, et al., J. Mater. Chem. A 7 (2019) 12842–12850.
[29] Y. Wu, M. Jing, J. Li, et al., Chin. Chem. Lett. 35 (2024) 109269.
[30] W. Deng, T. Wu, Y. Wu, et al., J. Mater. Chem. A 10 (2022) 20993–21003.
[31] T.F. Yi, L.Y. Qiu, J. Mei, et al., Sci. Bull. 65 (2020) 546–556.
[32] Y. Dong, Y. Feng, J. Deng, et al., Chin. Chem. Lett. 31 (2020) 909–914.
[33] H. Chang, Y.F. Guo, X. Liu, et al., Appl. Catal. B: Environ. 327 (2023) 122469.
[34] H. Chang, L. Zhao, S. Zhao, et al., J. Energy Chem. 93 (2024) 400–410.
[35] W. Xia, Z. Hou, J. Tang, et al., Nano Energy 94 (2022) 106868.
[36] R. Song, S. Zhang, Y. He, et al., Appl. Surf. Sci. 612 (2023) 155771.
[37] J. Xiao, Y. Zhang, T.C. Zhang, et al., Appl. Surf. Sci. 635 (2023) 157735.
[38] Q. Yang, Z. Tai, Q. Xia, et al., J. Mater. Chem. A 9 (2021) 8378–8385.
[39] L. Wu, M. Yang, L. Yao, et al., ACS Appl. Mater. Interfaces 14 (2022) 53947–53959.
[40] H. Chang, X. Liu, S. Zhao, et al., Adv. Funct. Mater. 34 (2023) 2313491.
[41] S. Sharma, V. Manchala, R. Gopalan, et al., Carbon 226 (2024) 119158.
[42] L. Suo, J. Zhu, X. Shen, et al., Carbon 151 (2019) 1–9.
[43] J. Liang, Z. Wei, C. Wang, et al., Electrochim. Acta 285 (2018) 301–308.